DOI: 10.1002/ejic.201000010

Origin of CO_3^{2-} Shortage in MgAl Layered Double Hydroxides with Mg/Al < 2

Shulan Ma,[a] Cuihong Fan,[a] Gailing Huang,[a] Yumei Li,[a] Xiaojing Yang,*[a] and Kenta Ooi[b]

Keywords: Layered compounds / Homogeneous precipitation / Hydrolysis / Magnesium / Aluminum

A carbonate shortage phenomenon (CO_3^{2-}/Al < 0.5) was found in MgAl layered double hydroxides (LDHs) with Mg/Al < 2 synthesized by the homogeneous precipitation (urea hydrolysis) method. To explain the phenomenon, a "gibbsite-layer based substitution–filling" model containing octahedral vacancies with formula $[Mg_y\square_{0.5-y}][Mg_xAl_{1-x}](OH)_3(CO_3^{2-})_{y-x/2}\cdot mH_2O$ is proposed on the basis of the detailed composition analysis and ordered distribution of Mg and Al in the layer.

Introduction

Layered double hydroxides (LDHs) have been attracting extensive attention because of their wide applications as anion exchangers,[1] catalysts,[2] bioactive[3] and electroactive materials,[4] and so on. LDHs have the general formula $[M^{II}_{1-x}M^{III}_x(OH)_2]^{x+}(A^{n-}_{x/n})\cdot mH_2O$, where x is normally in the range 0.20–0.33,[5] corresponding to M^{II}/M^{III} ratios of 4–2. By using the homogeneous precipitation method (by urea[6] or hexamethylenetetraamine (HMT)[7] hydrolysis), however, MgAl LDHs with Mg/Al ratios less than 2 (so-called Al-rich LDHs)[6b–6d] were often obtained, and also CO_3^{2-}/Al ratios were usually lower than the stoichiometric value of 0.5.[6c,6d] Another LDH (LiAl LDH) synthesized by this method also exhibited Li/Al and CO_3^{2-}/Li ratios less than the stoichiometric value of 0.5 based on the general formula $[LiAl_2(OH)_6](A^{n-}_{1/n})\cdot mH_2O$.[6e] The small Mg/Al ratio is considered to result from the higher solubility of magnesium hydroxide relative to that of aluminum hydroxide at low pH during urea hydrolysis,[6b,6d,8] whereas the CO_3^{2-} "shortage" is not structurally clear. On the basis of diffraction techniques,[6b,9] it is difficult to clarify the distribution of Mg and Al ions in the layer, and therefore, the CO_3^{2-} shortage. Recently, Grey et al.,[10] by means of solid-state NMR spectroscopy, revealed an ordered distribution of Mg and Al in the layers for LDHs having Mg/Al = 2 and a nonrandom distribution for those with Mg/Al > 2. However, for LDHs with Mg/Al < 2, there has been lack of a description of their structure. The CO_3^{2-} shortage implies a structure different from the "perfect" brucite layer. In this work, we carried out a detailed compositional and structural investigation for this kind of LDHs and proposed a structural model to explain the CO_3^{2-} shortage.

Results and Discussion

The XRD observations show that the sample obtained after a short time (30 min) at 140 °C (referred to as L140-30m, numbers being the reaction temperature and time) has peaks centered at the 2θ positions characteristic of aluminum hydroxide gel (Figure 1a),[6c,12] while it has a complicated composition (Table 1) indicated by the fact that Al/3OH > 1 and by the presence of NO_3^-, CO_3^{2-}, and H_2O. For a longer reaction time (Figure 1b), the peaks of Al(OH)$_3$ phases appear in addition to those of the LDH: the d value of 4.35 Å, (001) plane, is the basal spacing of Al(OH)$_3$, and the d values of 4.79 and 4.70 Å are assigned to the (010) plane of nordstrandite and (020) plane of bayerite (Figure 2),[13] respectively. All the XRD peaks of L140-50m (Figure 1c) can be indexed to have a hexagonal symmetry [a = 3.0317(3) Å and c = 22.520(3) Å], indicating a single phase, and the peaks of Al(OH)$_3$ disappear. The SEM observations (Figure 3) show that L140-40m has an irregular shape, L140-50m has plate-like uniform morphology, and increasing reaction time increases the crystallinity. Observations at 120, 100 (Figures 1e–g), and 80 °C (Figure S1) indicate that the reaction becomes slower at lower temperatures. Chemical analysis (Table 1) shows that the Mg/Al ratio increases gradually with reaction time; at 140 °C it reaches 2 for a reaction time of 24 h, suggesting the system goes to x = 0.33 as a stable phase, but at 100 °C, it hardly reaches 2, even though sharp and strong peaks in the XRD pattern (Figure 1j) and hexagonal prism mor-

[a] College of Chemistry, Beijing Normal University, Beijing 100875, China
Fax: +86-10-5880-2075
E-mail: yang.xiaojing@bnu.edu.cn
mashulan@bnu.edu.cn
[b] National Institute of Advanced Industrial Science and Technology, 2217-14 Hayashi, Takamatsu 761-0395, Japan
Fax: +81-87-869-3554
E-mail: k-ooi@aist.go.jp

Supporting information for this article is available on the WWW under http://dx.doi.org/10.1002/ejic.201000010.

phology in the SEM image (Figure 3h) were observed. In most samples, the ratios $CO_3^{2-}/Al < 0.5$, expected for the brucite-based structure (referred to as "brucite-based substitution model"), are observed, which indicates CO_3^{2-} shortage.

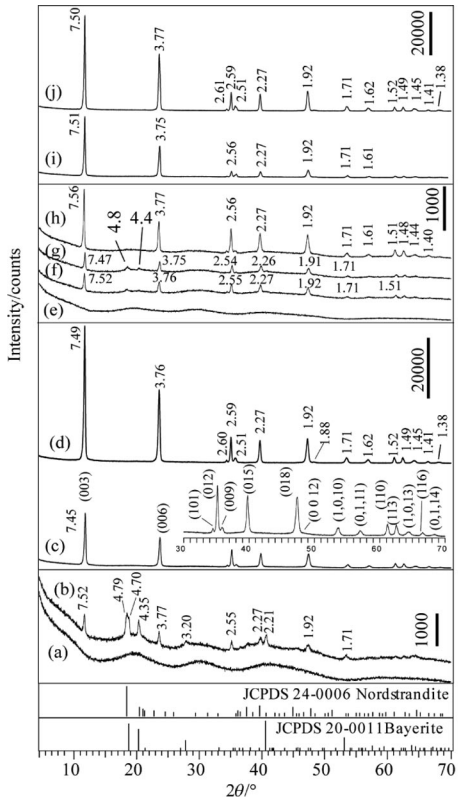

Figure 1. XRD patterns of the products hydrothermally reacted at 140 °C (a–d) for 30, 40, 50 min and 12 h, and at 100 °C (e–j) for 4, 5, 6, 7, 8, and 96 h, respectively (*d* values in Å).

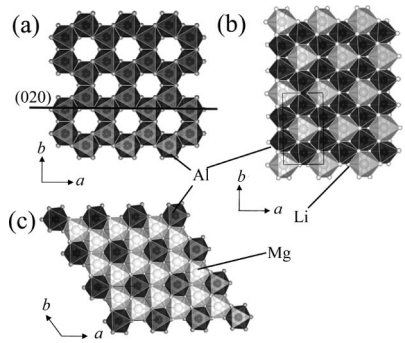

Figure 2. Schematic presentation of (a) bayerite, (b) LiAl LDH, and (c) MgAl LDH sheets.

The FTIR spectra (Figure 4) show that aluminum hydroxide containing a large quantity of nitrate [$\nu(NO_3^-)$: 1385 cm^{-1}] is produced at first; the same result was reported in the literature.[6c] At this point, the nitrate and carbonate ions may exist as aluminum-containing salts, that is, $Al_2(CO_3)_3$ and $Al(NO_3)_3$. This is further proved by the composition of the L140-30m sample with a Mg content of zero, whose formula can be written as $Al(OH)_3 \cdot 0.03Al_2(CO_3)_3 \cdot 0.02Al(NO_3)_3 \cdot 0.5H_2O$. Following the increase in the reaction time, the nitrate ions are progressively replaced by carbonate ions, which is testified by the absorption bands observed at 1356 (ν_{C-O}) and 781 (δ_{C-O}) cm^{-1} after 8 h.[6d] Moreover, the appearance of the bands at 692 (ν_{O-M}) and 449 cm^{-1} (δ_{O-M-O}), characteristic of lattice vibrations of [Mg, Al] octahedral sheets, shows evidence of the crystallization of the LDH phase.

The TG-DSC curves (Figure 5) show the formation process and the different forms of the LDHs at various temperatures. From 50–500 °C, the amorphous aluminum hydroxide (L140-30m) has only an endothermic peak at 90 °C, corresponding to the removal of water physically adsorbed

Table 1. Compositions for products at different temperatures and time.

T /°C	Time	Sample code	Mg/Al	CO_3^{2-}/Al	CO_3^{2-}/Mg	Chemical formula	Parameters[a]		
							x	*y*	% RVF
140	30 min	L140-30m	0.00	–	–	$Al_{1.08}(OH)_3(CO_3)_{0.09}(NO_3)_{0.06} \cdot 0.5H_2O$[b]	–	–	–
	40 min	L140-40m	0.04	–	–	$Mg_{0.04}Al_{1.05}(OH)_3(CO_3)_{0.11}(NO_3)_{0.008} \cdot 0.6H_2O$	–	–	–
	50 min	L140-50m	0.81	0.29	0.36	$Mg_{0.34}\square_{0.16}(Mg_{0.26}Al_{0.74})(OH)_3(CO_3)_{0.22} \cdot 1.0H_2O$	0.26	0.34	89
	2 h	L140-2h	1.63	0.46	0.28	$Mg_{0.47}\square_{0.03}(Mg_{0.44}Al_{0.56})(OH)_3(CO_3)_{0.26} \cdot 1.2H_2O$	0.44	0.47	98
	4 h	L140-4h	1.75	0.48	0.28	$Mg_{0.49}\square_{0.01}(Mg_{0.46}Al_{0.54})(OH)_3(CO_3)_{0.26} \cdot 1.1H_2O$	0.46	0.49	99
	12 h	L140-12h	1.82	0.48	0.26	$Mg_{0.49}\square_{0.01}(Mg_{0.47}Al_{0.53})(OH)_3(CO_3)_{0.25} \cdot 0.8H_2O$	0.47	0.49	99
	24 h	L140-24h	2.00	0.50	0.25	$Mg_{0.50}\square_{0.0}(Mg_{0.50}Al_{0.50})(OH)_3(CO_3)_{0.25} \cdot 0.7H_2O$	0.50	0.50	100
100	4 h	L100-4h	0.05	–	–	$Mg_{0.06}Al_{1.21}(OH)_3(CO_3)_{0.18}(NO_3)_{0.38} \cdot 2.1H_2O$	–	–	–
	5 h	L100-5h	0.09	–	–	$Mg_{0.09}Al_{1.03}(OH)_3(CO_3)_{0.13}(NO_3)_{0.01} \cdot 2.5H_2O$	–	–	–
	6 h	L100-6h	0.08	–	–	$Mg_{0.08}Al_{1.02}(OH)_3(CO_3)_{0.11}(NO_3)_{0.006} \cdot 1.6H_2O$	–	–	–
	7 h	L100-7h	0.24	0.15	0.61	$Mg_{0.17}\square_{0.33}(Mg_{0.06}Al_{0.94})(OH)_3(CO_3)_{0.14} \cdot 1.3H_2O$	0.06	0.17	78
	8 h	L100-8h	0.50	0.21	0.42	$Mg_{0.26}\square_{0.24}(Mg_{0.16}Al_{0.84})(OH)_3(CO_3)_{0.18} \cdot 1.4H_2O$	0.16	0.26	84
	12 h	L100-12h	0.80	0.29	0.36	$Mg_{0.35}\square_{0.15}(Mg_{0.25}Al_{0.75})(OH)_3(CO_3)_{0.22} \cdot 1.0H_2O$	0.25	0.35	90
	24 h	L100-24h	1.26	0.37	0.29	$Mg_{0.42}\square_{0.08}(Mg_{0.37}Al_{0.63})(OH)_3(CO_3)_{0.23} \cdot 0.8H_2O$	0.37	0.42	95
	34 h	L100-34h	1.44	0.41	0.29	$Mg_{0.45}\square_{0.05}(Mg_{0.41}Al_{0.59})(OH)_3(CO_3)_{0.25} \cdot 1.1H_2O$	0.41	0.45	97
	48 h	L100-48h	1.54	0.45	0.29	$Mg_{0.47}\square_{0.03}(Mg_{0.42}Al_{0.58})(OH)_3(CO_3)_{0.26} \cdot 1.4H_2O$	0.42	0.47	98
	72 h	L100-72h	1.60	0.47	0.29	$Mg_{0.48}\square_{0.02}(Mg_{0.43}Al_{0.57})(OH)_3(CO_3)_{0.27} \cdot 1.1H_2O$	0.43	0.48	99
	96 h	L100-96h	1.57	0.46	0.29	$Mg_{0.48}\square_{0.02}(Mg_{0.43}Al_{0.57})(OH)_3(CO_3)_{0.26} \cdot 0.9H_2O$	0.43	0.48	99

[a] *x* and *y* values are from the formula $[Mg_y\square_{0.5-y}][Mg_xAl_{1-x}](OH)_3(CO_3^{2-})_{y-x/2} \cdot mH_2O$. The rate of vacancy filled (RVF) is from $100(1 + y)/1.5$. [b] The composition can be written as $Al(OH)_3 \cdot 0.03Al_2(CO_3)_3 \cdot 0.02Al(NO_3)_3 \cdot 0.5H_2O$.

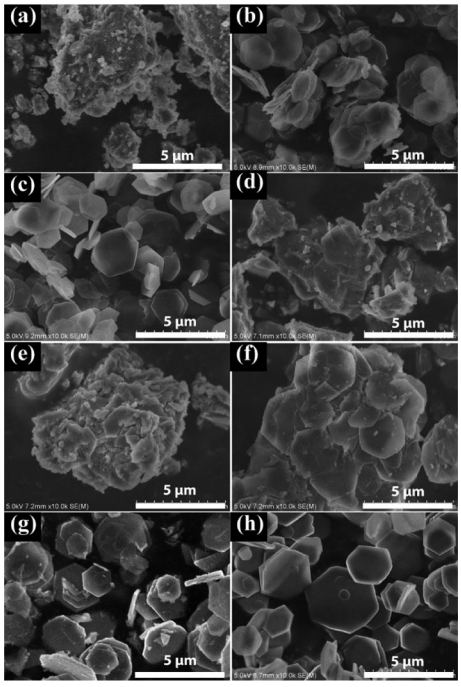

Figure 3. SEM images of the samples obtained at 140 °C (a–c) for 40, 50 min, and 12 h, and at 100 °C (d–h) for 6, 7, 8, 24, and 96 h, respectively.

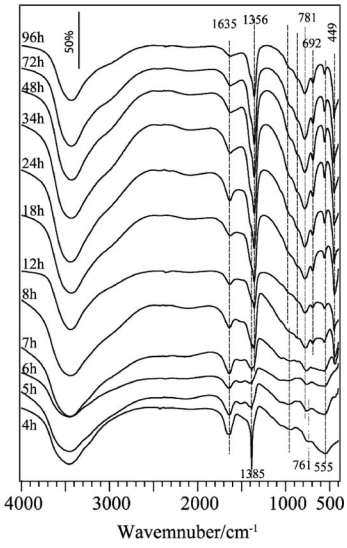

Figure 4. FTIR spectra of the samples reacted at 100 °C for different lengths of time.

to the surface. The LDH phases that have $Al(OH)_3$ peaks, L140-40m and L100-6h, have similar DSC curves; both curves have two endothermic peaks (at 64 and 99 °C for L140-40m, and 74 and 105 °C for L100-6h) corresponding to the removal of adsorbed water and two other endothermic peaks (at 184 and 249 °C for L140-40m and 195 and 260 °C for L100-6h), the former ones (184 and 195 °C) related to the removal of the interlayer water,[6b,6d] and the latter ones (249 and 260 °C) possibly due to the thermal decomposition of the $Al(OH)_3$ layers.[14] In the LDH samples after long-term reaction, the endothermic peaks at approximately 250 °C related to $Al(OH)_3$ disappear, indicating single LDH phases, and their TG-DSC curves have three endothermic peaks at around 200–234, 298–324, and approximately 450 °C, corresponding to the removal of interlayer water,[6b,6d] the dehydroxylation of the layer, and the interlayer decarbonation reactions, respectively.[6b,6d] The temperature of the second endothermic peak increased with the increase in Mg/Al ratios, showing the possible stronger interaction of metal ion and hydroxide on the layer.

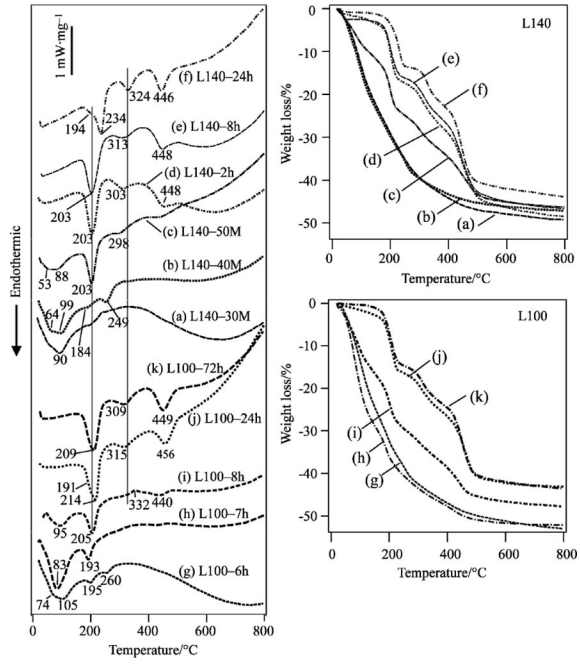

Figure 5. TG-DSC curves of the samples obtained at 100 and 140 °C by reaction for different lengths of time.

The structure of MgAl LDHs with Mg/Al < 2 as well as CO_3^{2-} shortage can not be simply elucidated by the conventional brucite-based substitution model, as the Al^{3+}–Al^{3+} close contacts not existing for Mg/Al ≥ 2[10] are unavoidable for Mg/Al < 2, because of the higher Al^{3+} content. Here, we propose a "gibbsite-based substitution–filling model" for the Al-rich LDHs, in analogy to the structure of LiAl LDH (Figure 2b). The $Al(OH)_3$-based (Figure 2a) filling model for LiAl LDH[13,15] can be used to present the structure of MgAl LDHs having all Al^{3+} located at the octahedral sites surrounded by $[Mg(OH)_6]$ octahedrons. In the present case, it is reasonable to think that domains of gibbsite[16]-like structure form at the initial stage of hydrolysis, since aluminum hydroxide precipitates preferentially at low pH. Due to the high Al^{3+} content, Al^{3+}–Al^{3+} close contacts will form at the gibbsite-like sheets, with octahedral vacancies. The LDH formation progresses with two reactions as (1) Mg^{2+} substitutes Al^{3+} to destroy the Al^{3+}–Al^{3+} contacts and (2) Mg^{2+} enters the octahedral vacancy with-

out surrounding Al^{3+}–Al^{3+} contacts. These reactions may progress simultaneously, and the final result of the substitution and filling is the formation of a brucite-layer structure with an ordering distribution of Mg and Al (Mg/Al = 2).

The formula based on the new model is given as $[Mg_y\square_{0.5-y}][Mg_xAl_{1-x}](OH)_3(CO_3^{2-})_{y-x/2}{\cdot}mH_2O$, in which y and x are the fraction of Mg filling the vacancies and that substituting "skeletal" Al, respectively. Based on this model, in the skeletal part $[Mg_xAl_{1-x}]$, Mg/Al = 1 is necessary for all vacancies to be filled up by other Mg^{2+}, leading to a typical brucite-layer structure as shown in Figure 2c. The content of CO_3^{2-} ($y - x/2$) is related to that of Mg^{2+} filling vacancies and substituting Al^{3+}. The substitution of Mg^{2+} for Al^{3+} leads to a decrease in the layer charge, and therefore the CO_3^{2-} content. The rate of vacancy filled (RVF, Table 1) can be calculated from $100(1 + y)/1.5$, where 1.5 is the total number of vacancies (0.5) and skeletal cations (1.0). The chemical formulae calculated from this model are listed in Table 1, and the calculated contents of the elements agree well with measured ones (Table S1). The RVF values increase with the reaction time, and when Mg/Al = 2, the vacancies are completely filled (RVF = 100%), as shown for L140-24h. The relation between the vacancy number (a) and the Al^{3+}–Al^{3+} close connect number (b) can be deduced to be $a \approx 0.75\ b$ (related coefficient, 0.987) by linear regression from the compositions. That is, one Al^{3+}–Al^{3+} close connect gives a vacancy, but the vacancy number does not equal the increase in Al content but is less. It should be noted that the present model can be applied to specific preparation routes like the urea hydrolysis method, where the precipitation of metal ions (Al^{3+} and Mg^{2+}) does not progress simultaneously, which is different from the case of the co-precipitation method, but progresses stepwise, first Al^{3+} followed by Mg^{2+} hydrolysis at different pH. In addition, the model might not be applicable for systems containing other divalent cations such as Zn, Ni, and Co. For example, the Ni^{2+}/Al^{3+} ratio in the NiAl LDH solid was found to be larger than that in the starting solution.[17]

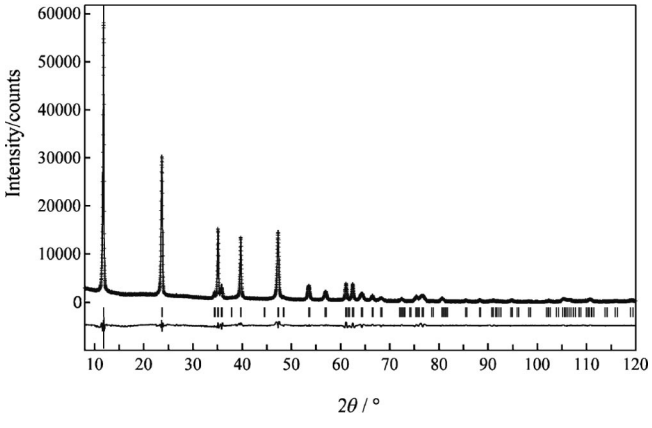

Figure 6. Rietveld refinement plots for the L100-24h sample. The experimental and simulated intensity data are plotted as dotted and solid lines, respectively; the line at the bottom is their intensity difference. The tick marks indicate the positions of all possible Bragg reflections from the structure model.

Since the XRD patterns of LDHs show no peaks of $Al(OH)_3$ (Figure 1c, i, and j), the vacancy distribution would be random or the amount is low. The vacancy presence is testified by Rietveld refinement of the pattern of L100-24h. Figure 6 shows that the calculated pattern coincides well with the measured one, indicating that the model employed (Table S2) can be used to describe the structure. The bond lengths of 2.0123(9) and 3.0353(3) Å for Mg(Al)–O and Mg(Al)–Mg(Al), respectively, are among the ranges but close to the small end of those reported for LDHs with Mg/Al = 2. In this model, the RVF was set to be 94%, as shown by the occupancies of 0.51 and 0.43 for Mg and Al, respectively (Table S2).

Conclusions

The structure of Al-rich MgAl LDHs can be represented by a "substitution–filling model", $[Mg_y\square_{0.5-y}][Mg_xAl_{1-x}](OH)_3(CO_3^{2-})_{y-x/2}{\cdot}mH_2O$, based on the gibbsite-like layer, where Al^{3+}–Al^{3+} close contacts would give octahedral vacancies. Mg^{2+} substitution for skeletal Al^{3+} and filling of the vacant octahedral holes both take place. The presence of the vacancies well accounts for the apparent CO_3^{2-} shortage and reveals a structural feature of a new kind of LDH. The present structure and model on the LDH may give useful information for the studies concerning LDH chemistry, such as catalysis,[2] intercalation, shape-selective ion exchange,[18] and the recently highlighted exfoliation.[19]

Experimental Section

Iyi et al.[11] used three [Mg + Al] concentrations of 0.15, 0.075, and 0.1875 M and varied urea/Al molar ratios from 1.75 to 12 at 140 °C to study the formation of MgAl LDH by the homogeneous precipitation method. According to the literature,[11] we synthesized the samples by fixing the Mg/Al molar ratio to 2, the [Mg+Al] concentration to 0.15 M, and the urea/Al molar ratio to 10, but changing temperatures from 80 to 140 °C. In detail, $Mg(NO_3)_2{\cdot}6H_2O$ (1.28 g), $Al(NO_3)_2{\cdot}9H_2O$ (0.95 g), and urea (1.50 g) were dissolved in deionized water to yield a 50 cm^3 solution of 0.1 M, 0.05 M, and 0.5 M, respectively. The pH value of the starting solution, determined at room temperature, was 3.4. The mixed solution was hydrothermally treated in a 100 cm^3 Teflon autoclave at the set temperature. After being heated for a known time interval and cooled at ambient temperature, the solid was centrifuged, washed with water, and dried at 40 °C for 24 h in vacuo. The final pH values, measured after the reacted solutions were cooled to room temperature, gradually increased from 6.8 (for 4 h) to 8.5 (for 96 h) at 100 °C, and from 6.4 (for 30 min) to 9.5 (for 12 h) at 140 °C. The actual pH values in the autoclave would be lower than those measured at room temperature, according to the literature.[6c] The samples were subjected to XRD measurement with a Phillips X'pert Pro MPD diffractometer. The Mg and Al contents were analyzed by ICP atomic emission spectroscopy (Jarrel-ASH, ICAP-9000) after the solid sample was dissolved in an HCl solution, and C, H and N contents were determined by using an Elementar Vario EL elemental analyzer. Chemical formulas for these products were calculated by assuming the content of OH, which, along with CO_3^{2-} and NO_3^-, was charge-balanced to Mg^{2+} and Al^{3+}. TG-DSC mea-

surement was performed with a NETZSCH STA 409 PC/PG thermal analyzer, FTIR spectroscopy was performed with a Nicolet-380 Fourier-transform infrared spectrometer, and FE-SEM analysis was conducted with a mode S-4800 (Hitachi, Ltd.) instrument operating at 5.0 kV.

Supporting Information (see footnote on the first page of this article): XRD patterns of the products reacted at 80 °C, ICP and CHN analysis data, structural parameters for the L100-24h sample.

Acknowledgments

This work is supported by the National Science Foundation of China (20671012, 50872012, and 20871018).

[1] S. P. Newman, W. Jones, *New J. Chem.* **1998**, *22*, 105–115.
[2] S. Hamada, K. Ikeue, M. Machida, *Chem. Mater.* **2005**, *17*, 4873–4879.
[3] a) J. H. Choy, S. Y. Kwak, J. S. Park, Y. J. Jeong, J. Portier, *J. Am. Chem. Soc.* **1999**, *121*, 1399–1400; b) J. H. Choy, S. Y. Kwak, Y. J. Jeong, J. S. Park, *Angew. Chem. Int. Ed.* **2000**, *39*, 4042–4045; c) J. H. Choy, S. Y. Kwak, J. S. Park, Y. J. Jeong, *J. Mater. Chem.* **2001**, *11*, 1671–1674.
[4] a) J. Tronto, K. C. Sanchez, E. L. Crepaldi, Z. Naal, S. I. Klein, J. B. Valim, *J. Phys. Chem. Sol.* **2004**, *65*, 493–498; b) B. Mavis, M. Akinc, *J. Power Sources* **2004**, *134*, 308–317; c) J. Qiu, G. Villemure, *J. Electroanal. Chem.* **1997**, *428*, 165–172.
[5] F. Cavini, F. Trifiro, A. Vaccari, *Catal. Today* **1991**, *11*, 173–301.
[6] a) H. Cai, A. C. Hiller, K. R. Franklin, C. C. Nunn, M. D. Ward, *Science* **1994**, *266*, 1551–1555; b) U. Costantino, F. Marmottini, M. Nocchetti, R. Vivani, *Eur. J. Inorg. Chem.* **1998**, 1439–1446; c) M. Adachi-Pagano, C. Forano, J.-P. Besse, *J. Mater. Chem.* **2003**, *13*, 1988–1993; d) M. Ogawa, H. Kaiho, *Langmuir* **2002**, *18*, 4240–4242; e) E. Narita, Y. Matsuno, S. Takahashi, Y. Umetsu, *Niika* **2001**, *5*, 273–279. (in Japanese).
[7] a) N. Iyi, T. Matsumoto, Y. Kaneko, K. Kitamura, *Chem. Lett.* **2004**, *33*, 1122–1123; b) N. Iyi, K. Okamoto, Y. Kaneko, T. Matsumoto, *Chem. Lett.* **2005**, *34*, 932–934.
[8] U. Unal, *J. Solid State Chem.* **2007**, *180*, 2525–2533.
[9] a) M. Bellotto, B. Rebours, O. Clause, J. Lynch, D. Bazin, E. Elkaim, *J. Phys. Chem.* **1996**, *100*, 8527–8534; b) G. R. Williams, D. O'Hare, *Chem. Mater.* **2005**, *17*, 2632–2640.
[10] P. J. Sideris, U. G. Nielsen, Z. Gan, C. P. Grey, *Science* **2008**, *321*, 113–117.
[11] K. Okamoto, N. Iyi, T. Sasaki, *Appl. Clay Sci.* **2007**, *37*, 23–31.
[12] M. Inoue, Y. Kondo, T. Inui, *Chem. Lett.* **1986**, 1421–1424.
[13] S. Britto, G. S. Thomas, P. V. Kamath, S. Kannan, *J. Phys. Chem. C* **2008**, *112*, 9510–9515.
[14] W. Tongamp, Q. Zhang, F. Saito, *J. Mater. Sci.* **2007**, *42*, 9210–9215.
[15] a) A. V. Besserguenev, A. M. Fogg, R. J. Francis, S. J. Price, D. O'Hare, V. P. Isupov, B. P. Tolochko, *Chem. Mater.* **1997**, *9*, 241–247; b) A. M. Fogg, A. J. Freij, G. M. Parkinson, *Chem. Mater.* **2002**, *14*, 232–234; c) G. R. Williams, A. J. Norquist, D. O'Hare, *Chem. Mater.* **2004**, *16*, 975–981.
[16] We use gibbsite instead of bayerite or nordstrandite to describe the intralayer because the present MgAl LDH has a hexagonal symmetry, which is the same as that of LiAl LDH. For the latter, the symmetry is usually obtained from gibbsite [γ-$Al(OH)_3$],[15a] whilst that of its rhombohedral polymorph from bayerite or nordstrandite as precursors.[15b]
[17] B. Mavis, M. Akinc, *Chem. Mater.* **2006**, *18*, 5317–5325.
[18] a) F. Millange, R. I. Walton, L. X. Lei, D. O'Hare, *Chem. Mater.* **2000**, *12*, 1990–1994; b) A. I. Khan, D. O'Hare, *J. Mater. Chem.* **2002**, *12*, 3191–3198; c) D. G. Evans, X. Duan, *Chem. Commun.* **2006**, 485–496.
[19] a) Z. P. Liu, R. Z. Ma, M. Osada, N. Iyi, Y. Ebina, K. Takada, T. Sasaki, *J. Am. Chem. Soc.* **2006**, *128*, 4872–4880; b) R. Z. Ma, Z. P. Liu, K. Takada, N. Iyi, Y. Bando, T. Sasaki, *J. Am. Chem. Soc.* **2007**, *129*, 5257–5263.

Received: January 6, 2010
Published Online: April 12, 2010

